Available online at www.sciencedirect.com
ScienceDirect
Journal of Magnetic Resonance 192 (2008) 209–217
JMR Journal of Magnetic Resonance
www.elsevier.com/locate/jmr

Compensation of gradient-induced magnetic field perturbations

Terence W. Nixon, Scott McIntyre, Douglas L. Rothman, Robin A. de Graaf *

Departments of Diagnostic Radiology and Biomedical Engineering, Magnetic Resonance Research Center, Yale University, School of Medicine, TAC, N145, 300 Cedar Street, P.O. Box 208043, New Haven, CT 06520-8043, USA

Received 21 November 2007; revised 20 February 2008
Available online 23 February 2008

Abstract

Pulsed magnetic field gradients are essential for MR imaging and localized spectroscopy applications. However, besides the desired linear field gradients, pulsed currents in a strong external magnetic field also generate unwanted effects like eddy currents, gradient coil vibrations and acoustic noise. While the temporal magnetic field perturbations associated with eddy currents lead to spectral line shape distortions and signal loss, the vibration-related modulations lead to anti-symmetrical sidebands of any large signal (i.e. water), thereby obliterating the signals from low-concentration metabolites. Here the measurement, characterization and compensation of vibration-related magnetic field perturbations is presented. Following a quantitative evaluation of the various temporal components of the main magnetic field, a digital B_0 magnetic field waveform is generated which reduces all temporal variations of the main magnetic field to within the spectral noise level.

Keywords: Gradient coil vibration; Temporal magnetic field variation; Vibration-related sidebands; Water suppression; Non-water-suppressed NMR

1. Introduction

Pulsed magnetic field gradients are an essential part of almost all MRI and localized MRS methods. However, the generation of magnetic field gradients requires time-varying currents which, in the presence of a strong external magnetic field, can lead to a number of unwanted effects like eddy currents [1–3], gradient coil vibrations [4] and acoustic noise [5–7]. Eddy currents are a manifestation of Faraday's law of induction in which a time-varying magnetic field will induce a current in any nearby conducting structure, like the cryostat. The magnetic field associated with the eddy currents will oppose the effect of the applied time-varying magnetic field. The effects of eddy currents can typically be seen as line shape distortions and signal loss in MRS [8,9] and geometric distortion in MRI [10]. Since the effects of eddy currents are well-recognized, all commercial MR systems are equipped with exponential B_0 compensation and gradient pre-emphasis circuits on the gradient input signal in order to minimize the eddy current effects on the gradient output signal [1–3].

Gradient coil vibrations and acoustic noise are caused by Lorentz forces acting on the gradient coil windings during a time-varying current [4]. The gradient coil windings, and as a consequence the entire gradient coil former, are deformed during a gradient pulse and relax back to their original state in an damped, oscillatory fashion [4]. While the exact mechanism is not well understood, the gradient coil vibrations do lead to damped sinusoidal perturbations of the main magnetic field B_0. The temporal variations in B_0 lead to phase variations in the acquired NMR signal which, following Fourier transformation, result in spurious resonances ('sidebands') symmetrically positioned around NMR resonances. Since the vibration-related sidebands typically only represent a small fraction (0–2%) of the NMR resonance, they are normally only visible on large NMR resonances like water [11] and lipids [12]. However, despite the relatively small amplitude, vibration-related sidebands largely prevent non-water-suppressed MRS and MRSI [11,13–16]. This is because the vibration-related sidebands typically overwhelm the NMR resonances from

* Corresponding author. Fax: +1 203 785 6643.
E-mail address: robin.degraaf@yale.edu (R.A. de Graaf).

1090-7807/$ - see front matter © 2008 Elsevier Inc. All rights reserved.
doi:10.1016/j.jmr.2008.02.016

the low-concentration metabolites. Non-water-suppressed MRS(I) is generally desirable as the large water resonance can be used for automated frequency and phase correction, internal concentration referencing and as an objective measure for selecting acceptable data from large MRSI datasets. However, since the gradient-induced magnetic field perturbations require tens of milliseconds to decay, non-water-suppressed MRS(I) only becomes practical at very long echo-times [17].

Here the measurement, theoretical characterization and experimental compensation of vibration-related magnetic field perturbations is presented. While some of the measurements and characterizations have been performed previously (e.g. [11]), this is the first report that provides a complete quantification and subsequent hardware-based compensation of vibration-related sidebands.

2. Theory

The phase of any acquired NMR signal can be analyzed for vibration-related modulations, under the assumption that the total measured phase can be decomposed into four separate contributions according to

$$\phi_{\text{total}}(t) = \phi_0 + \phi_{\text{frequency}}(t) + \phi_{\text{EC}}(t) + \phi_{\text{vibration}}(t) \tag{1}$$

whereby ϕ_0 is a constant, zero-order phase offset and $\phi_{\text{frequency}}$ a linearly varying phase proportional to a frequency offset $\Delta\nu$, i.e. $\phi_{\text{frequency}}(t)=2\pi\Delta\nu t$. ϕ_{EC} represents the phase evolution from exponentially decaying magnetic field perturbations associated with eddy currents and is given by:

$$\begin{aligned}\phi_{\text{EC}}(t) &= \gamma \int_0^t \sum_{n=1}^{N} B_{\text{EC},n} \mathrm{e}^{-t'/\text{TC}_{\text{EC},n}}\,\mathrm{d}t' \\ &= \gamma \sum_{n=1}^{N} B_{\text{EC},n}\text{TC}_{\text{EC},n}\left(1-\mathrm{e}^{-t/\text{TC}_{\text{EC},n}}\right)\end{aligned} \tag{2}$$

where $B_{\text{EC},n}$ and $\text{TC}_{\text{EC},n}$ are the amplitude (in T) and time constant (in s) for the temporal magnetic field perturbation associated with eddy current n. On most MR systems eddy currents can be compensated up to $N = 3$ or 4.

Finally, $\phi_{\text{vibration}}$ represents the phase evolution from magnetic field perturbations associated with vibrations and deformations of the gradient coils. Based on prior work [11] and the results presented in this manuscript it appears reasonable to describe the temporal magnetic field perturbations as damped sinusoidal functions according to:

$$B_{\text{vibration}}(t) = \sum_{n=1}^{N} B_{\text{vib},n}\cos(2\pi\nu_{\text{vib},n}t + \phi_{\text{vib},n})\mathrm{e}^{-t/\text{TC}_{\text{vib},n}} \tag{3}$$

where $B_{\text{vib,n}}$, $\nu_{\text{vib,n}}$, $\phi_{\text{vib,n}}$ and $\text{TC}_{\text{vib,n}}$ are the amplitude (in T), frequency (in Hz), initial phase (in radians) and time constant (in s) for the temporal magnetic field perturbation associated with vibration n. The phase $\phi_{\text{vibration}}$ is then given by:

$$\begin{aligned}\phi_{\text{vibration}}(t) = \gamma \sum_{n=1}^{N} & \frac{B_{\text{vib},n}\mathrm{e}^{-t/\text{TC}_{\text{vib},n}}}{(2\pi\nu_{\text{vib},n})^2 + (1/\text{TC}_{\text{vib},n})^2} \\ & \times \left[2\pi\nu_{\text{vib},n}\sin(2\pi\nu_{\text{vib},n}t + \phi_{\text{vib},n}) - \frac{\cos(2\pi\nu_{\text{vib},n}t + \phi_{\text{vib},n})}{\text{TC}_{\text{vib},n}}\right] \\ & - \frac{B_{\text{vib},n}}{(2\pi\nu_{\text{vib},n})^2 + (1/\text{TC}_{\text{vib},n})^2} \\ & \times \left[2\pi\nu_{\text{vib},n}\sin(\phi_{\text{vib},n}) - \frac{\cos(\phi_{\text{vib},n})}{\text{TC}_{\text{vib},n}}\right].\end{aligned} \tag{4}$$

Fig. 1A shows a graphical depiction of a vibration-related sideband as calculated with Eqs. (3) and (4) for $N = 1$, $B_{\text{vib}} = 0.25\ \mu\text{T}$, $\nu_{\text{vib}} = 300$ Hz, $\text{TC}_{\text{vib}} = 0.1$ s and $\phi_{\text{vib}} = 0$ or $\pi/2$. The primary spectral sidebands appear with opposite signs at ± 300 Hz and an amplitude of circa 0.9% of the on-resonance signal (Fig. 1A1). Changing the initial phase of the vibration-related phase modulation directly affects the phase of the spectral sidebands, but maintains the asymmetrical appearance (Fig. 1A3). While difficult to prove analytically (due to the presence of inte-

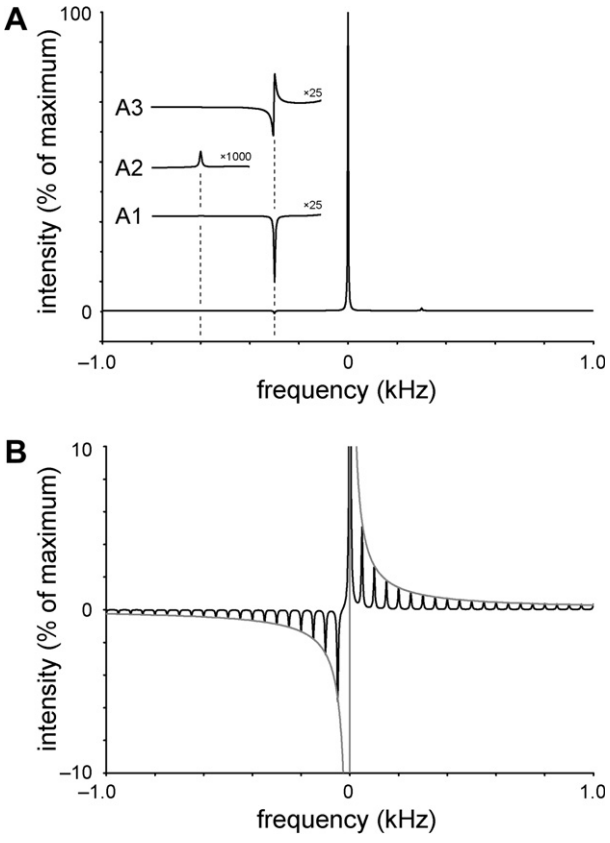

Fig. 1. Simulated spectral sidebands caused by damped, sinusoidal modulation of the main magnetic field. (A) Simulated spectral sideband for $B_{\text{vib}} = 0.25\ \mu\text{T}$, $\nu_{\text{vib}} = 300$ Hz, $\text{TC}_{\text{vib}} = 0.1$ s and (A1 and A2) $\phi_{\text{vib}} = 0$ or (A3) $\pi/2$. Using an expanded vertical scale, (A2) a second harmonic at $\nu_{\text{vib}} = 2 \times 300\ \text{Hz} = 600$ Hz can be seen. (B) Simulated spectral sidebands for $B_{\text{vib}} = 0.25\ \mu\text{T}$, $\text{TC}_{\text{vib}} = 0.1$ s and $\nu_{\text{vib}} = n{\cdot}50$ Hz ($n = 1$–20). The height of the sidebands is proportional to ν_{vib}^{-1} (gray line).

grals of the form $\int e^{\sin x} dx$), it can readily be shown numerically or approximately through a Taylor series expansion that sidebands also appear at integer multiples of the primary vibration frequency (Fig. 1A2). Even order sidebands typically appear symmetrical around the on-resonance signal, while the odd order sidebands (including the primary sidebands) appear anti-symmetrical. Especially for lower primary vibration frequencies (i.e. <100 Hz) the amplitude of the second harmonic can be up to a few percent of the primary sideband.

From Eqs. (3) and (4) it follows that for a constant amplitude B_{vib} and time constant TC_{vib}, the efficiency of generating sidebands at frequency v_{vib} scales proportional to $(1/v_{vib})$ (Fig. 1B). This is in good agreement with experimental observations (see Section 4) in which the most intense vibration-related sidebands are close to the water resonance.

3. Materials and methods

All experiments were performed on a 4.0 T Magnex magnet (Magnex Scientific Ltd, Oxford, UK) interfaced to a Bruker Avance Spectrometer (Bruker Instruments, Billerica, MA) equipped with Magnex gradients capable of switching 36 mT/m in 2.0 ms. RF transmission and reception was performed with an 8 cm diameter surface coil tuned to the proton NMR frequency (170.4 MHz).

Compensation of the temporal phase modulations *in vitro*, as well as *in vivo*, was performed on NMR signals acquired with a 3D localized NMR sequence based on the LASER method [18,19]. The LASER method was executed with an 0.75 ms adiabatic half passage (AHP, tanh/tan modulation, maximum frequency modulation $\Delta\omega_{max} = 50$ kHz) pulse for excitation, 6.0 ms adiabatic full passage (AFP, sech/tanh modulation, $\Delta\omega_{max} = 0.833$ kHz) pulses for refocusing and 1.2 ms 33 mT/m magnetic field crusher gradients, giving a minimum echo-time TE of 100 ms. The localized volume ($15 \times 15 \times 15$ mm = 3.38 mL) was placed in the magnetic isocenter. Water and metabolite spectra were acquired with 16 and 256 individually stored transients (TR = 3000 ms), which allowed frequency alignment prior to summation. Where applicable, water suppression was achieved with SWAMP [20], an adiabatic analog of CHESS [21].

Fig. 2 shows the principle for obtaining accurate digital compensation of temporal magnetic field distortions. All calculations were performed in Matlab 6.0 (The Mathworks, Natick, MA) running on a Linux PC. The real and imaginary parts of the acquired water signal (Fig. 2A) allow the calculation of a temporally varying

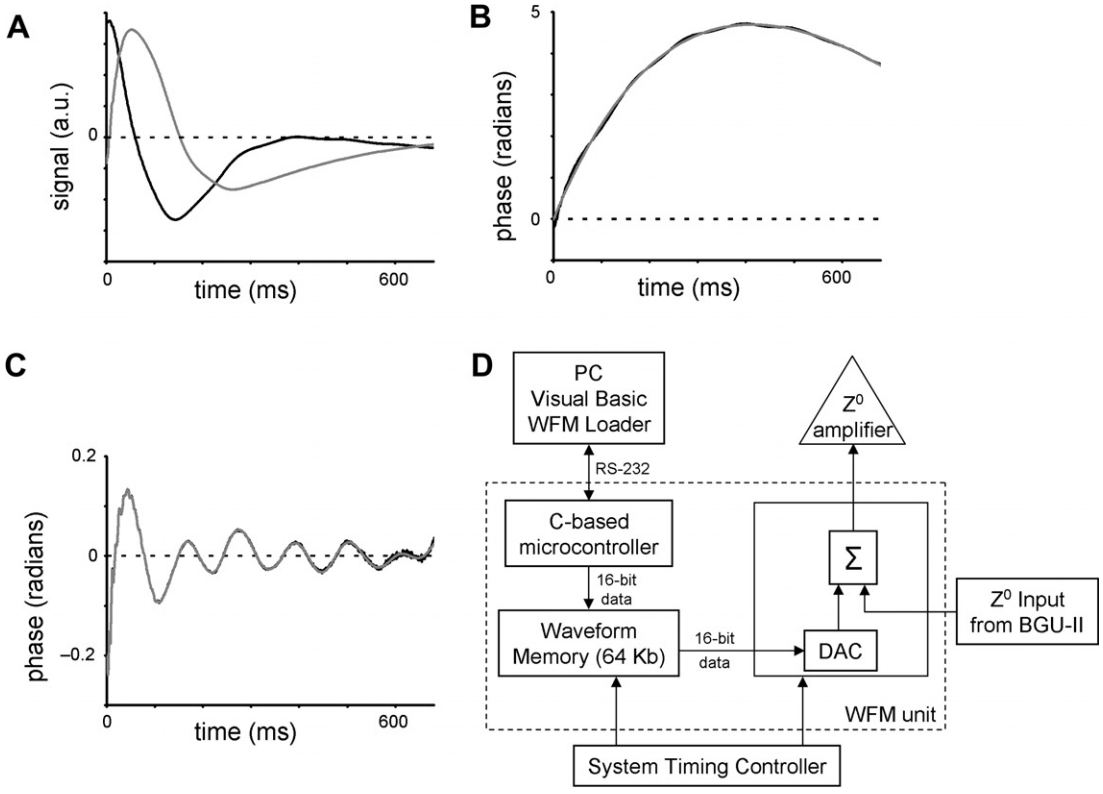

Fig. 2. Principle of compensating vibration-related phase modulations. (A) The real (black line) and imaginary (gray line) parts of a strong NMR signal, like water allows the calculation of (B) the temporal phase evolution (black line). Removing the constant (ϕ_0), linear ($\phi_{frequency}(t)$) and eddy current-related ($\phi_{EC}(t)$) phase modulations as obtained by least-square fitting (gray line) gives (C) the vibration-related phase modulations, $\phi_{vibration}(t)$ (black line). The opposite of the digital waveform approximating the vibration-related phase modulations according to Eq. (4) (gray line) is then stored into the local memory of the WFM unit (D). Specific timing controls within the pulse sequence strobe the digital waveform to the B_0 amplifier, where it counteracts the temporal magnetic field perturbations caused by gradient vibrations.

phase (Fig. 2B) which is typically fitted with $\phi(t)=\phi_0+\phi_{\text{frequency}}(t)+\phi_{\text{EC}}(t)$, with $N=5$ for $\phi_{\text{EC}}(t)$. The phase difference was assumed to be vibration-related phase modulations (Fig. 2C) and was fitted with $\phi(t)=\phi_{\text{vibration}}(t)$ with $N=40$–50. The fitted phase modulation was recalculated as 16-bit data at the time resolution of the waveform memory (WFM) unit, which was fixed at 50.048 μs. Following scaling for the B_0 coil efficiency of 1.25 μT/100% the digital waveform was transferred to the local memory of the WFM unit via a Visual Basic loading interface and a RS232 serial protocol. During the actual experiment, a pulse sequence command initiated the digital-to-analog (DAC) conversion of the digital waveform. Following summation with other B_0 magnetic field modulations coming from the Bruker Gradient Control Unit (BGU-II), the combined signal was sent to the B_0 magnetic field coil.

Characterization of the temporal and spatial phase modulations *in vitro* was performed on NMR signals acquired with a non-localized, pulse-acquire NMR sequence (250 μs square excitation pulse, TR = 3000 ms) using a surface coil for transmission and reception. Inherent spatial localization was provided by the small dimensions of the sample (water-filled sphere, radius = 10 mm) and the surface coil (radius = 8 mm). The pulse-acquire sequence was extended with a variety of magnetic field gradients prior to excitation (see Section 4 for more details) to verify the dependence of sidebands on the magnetic field gradient amplitude and timing. To test the dependence upon spatial position, the coil/sample assembly could be shifted in any of the three Cartesian directions.

4. Results

Fig. 3 shows ^{1}H NMR spectra acquired from a 3D localized volume (15 × 15 × 15 mm) *in vitro* without (gray line) and with (black line) compensation of gradient-induced magnetic field perturbations. Since *all* temporal phase modulations are compensated, including those from regular (residual) eddy currents, the spectral line shape significantly improves following compensation, closely approximating the theoretical Lorentzian line shape (Fig. 3A).

Without compensation strong vibration-related sidebands are visible at the spectral baseline with amplitudes as high as 1.5% of the main water signal at 0 Hz (Fig. 3B). Quantitatively, primary sidebands are present between 0 and 250 Hz, with typical decay constants of 10–50 ms and typical amplitudes of 0–0.4 μT. The highest vibration-related amplitude of 0.8 μT was encountered for the signal at circa 200 Hz. Significant vibration-related sidebands with amplitudes >0.1 μT were routinely observed for frequencies as high as 1.5 kHz. Therefore, in order to obtain satisfactory compensation, the temporal phase evolution was typically fitted with 40–50 damped sinusoids. Following compensation of vibration-related magnetic field perturbations (Fig. 3B, black line) the sidebands have been reduced to below the spectral noise level.

Fig. 4 shows localized ^{1}H NMR spectra acquired from the human occipital cortex at 4 T. Besides some minor residual line broadening from magnetic field inhomogeneity, the water resonance (Fig. 4A) is characterized by line shape distortions caused by residual, uncompensated eddy currents. Without water suppression the baseline is dominated by vibration-related sidebands (Fig. 4B), making reliable detection of metabolite resonances difficult. When the same NMR pulse sequence is executed in conjunction with damped sinusoidal B_0 compensation, the water resonance is characterized by a well-defined Lorentzian line shape (Fig. 4C). Furthermore, the vibration-related sidebands have been suppressed to below the spectral noise level, thus allowing direct detection of metabolite resonances (Fig. 4D). While the large water resonance and the associated sidebands can also be suppressed by water suppression techniques, the metabolite line shape distortions remain

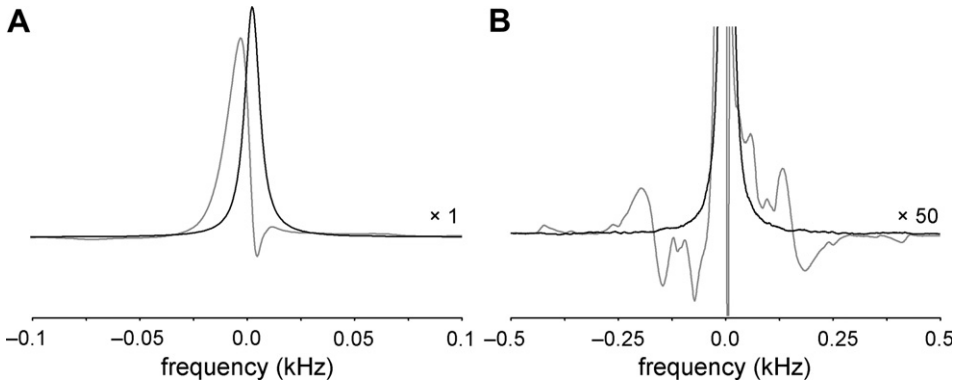

Fig. 3. *In vitro* evaluation of WFM-based compensation of vibration-related magnetic field perturbations. (A) Residual phase evolution due to uncompensated eddy currents leads to a distortion of the spectral line shape (gray line). When the digital waveform is played out during signal acquisition, the residual eddy current-related phase evolution is canceled, thereby leading to a near-perfect Lorentzian line shape (black line). (B) Expanding the vertical scale 50 times clearly shows the anti-symmetrical sidebands caused by vibration-related phase evolution (gray line). In the presence of a compensating B_0 magnetic field modulation as dictated by the digital waveform stored in the WFM unit, the sidebands are reduced to within the spectral noise level (black line).

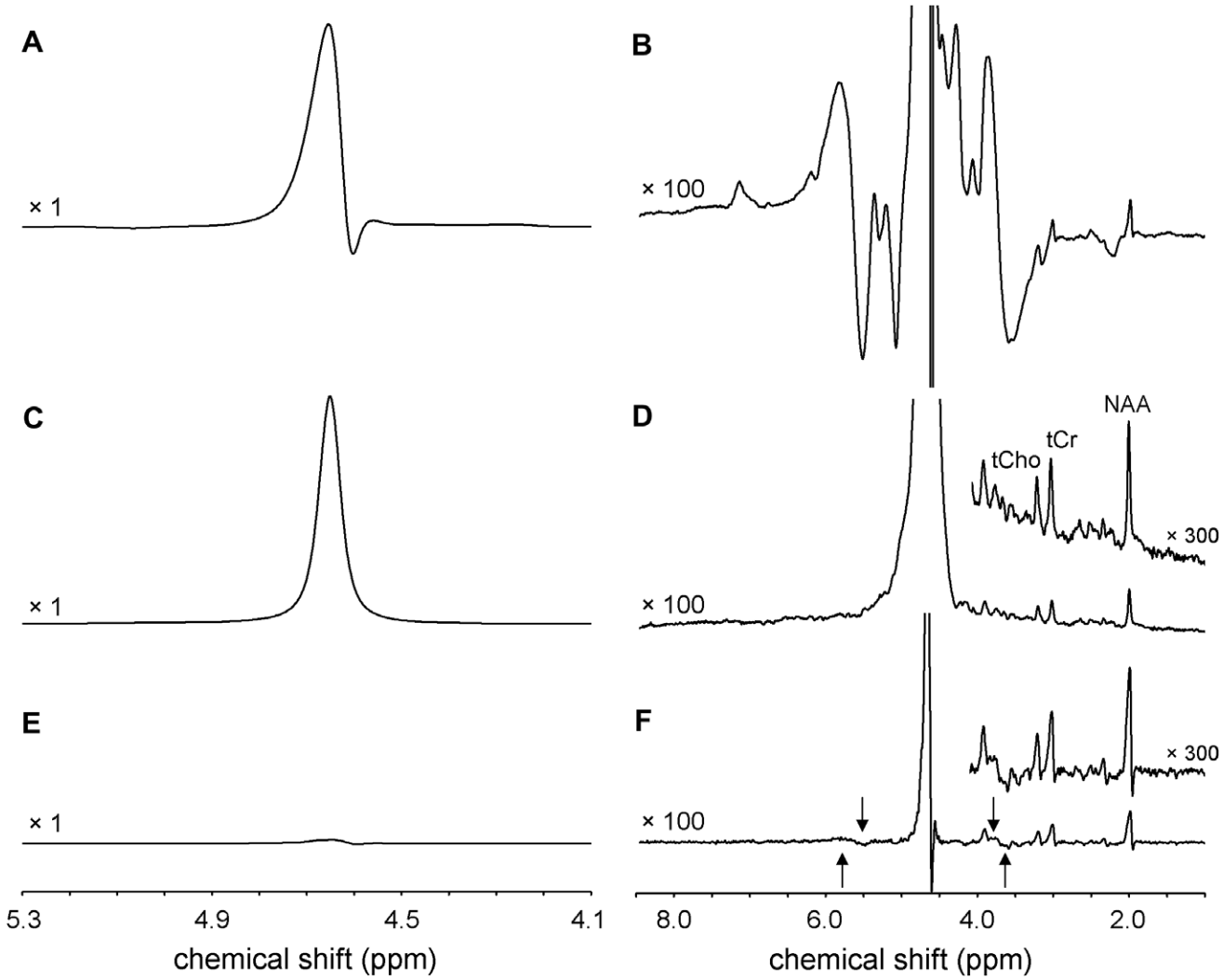

Fig. 4. *In vivo* evaluation of WFM-based compensation of vibration-related magnetic field perturbations. (A and B) Localized, non-water-suppressed ^{1}H NMR spectra from the human brain at 4 T in the *absence* of WFM-based B_0 magnetic field compensation. (A) Line shape distortions and (B) sidebands are clearly visible. (C and D) Localized, non-water-suppressed ^{1}H NMR spectra in the *presence* of WFM-based B_0 magnetic field compensation. The Lorentzian line shape has been restored, whereas the sidebands are suppressed to within the spectral noise level. (E and F) Localized, water-suppressed ^{1}H NMR spectra in the absence of WFM-based B_0 magnetic field compensation. While the absence of a large water signal has greatly reduced the vibration-related sidebands, the line shape distortions due to residual eddy currents remain. Furthermore, in the case of incomplete water suppression, small but coherent sidebands may become visible (arrows).

(Fig. 4F). Furthermore, in the presence of incomplete water suppression, small but coherent residual sidebands may still be present (Fig. 4F). Note that the damped sinusoidal B_0 compensation used for the *in vivo* experiments was obtained on an *in vitro* sample with the identical NMR pulse sequence and applied without further modification.

Figs. 3 and 4 have demonstrated the applicability of damped sinusoidal B_0 compensation using a predetermined B_0 waveform stored in local memory. However, this approach is highly pulse sequence specific and requires the determination of new compensation wave forms for each new NMR pulse sequence. A more general approach can be obtained when the B_0 compensation waveforms can be derived from the response of a single, normalized magnetic field gradient pulse.

Figs. 5–7 summarize the requirements, and their experimental verification, necessary for a general, sequence-independent implementation of damped sinusoidal B_0 compensation. First and foremost, the vibration-related sidebands scale linearly with the applied magnetic field gradient amplitude (Fig. 5A). Furthermore, part of the vibration-related sidebands scales approximately linearly with the distance from the magnet isocenter (Fig. 5B), indicating that complete compensation of vibration-related field perturbations will also require damped sinusoidal pre-emphasis of the linear gradients. Sidebands originating from 'cross terms' (e.g. sidebands originating from a gradient applied in the x direction observed at an off-center z position) were minimal and could be ignored. However, this could be gradient-coil-specific and should be verified for a given system.

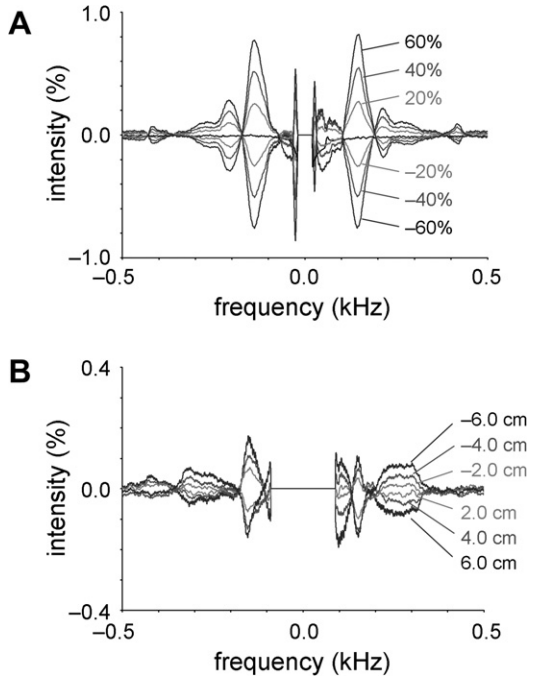

Fig. 5. Vibration-related sidebands as a function of (A) gradient amplitude and (B) spatial position. For all experiments, a 2 ms magnetic field gradient in the z direction was used, although similar results were obtained for magnetic field gradients in the x and y directions. The data in (A) was obtained in the magnetic isocenter for the gradient amplitude indicated. The spectral sidebands appear largely symmetrical with respect to the on-resonance water signal. Note that data is presented as the difference between measurements with $G \neq 0$ and $G = 0$. The residual on-resonance water signal has been set to zero in order to high-light the vibration sidebands. The data in (B) was obtained by mounting the sample at the indicated z positions in the presence of a +60% magnetic field gradient. The spectral sidebands appear largely anti-symmetrical with respect to the on-resonance water resonance. Note that data is presented as the difference between measurements at $z \neq 0$ and $z = 0$. The residual on-resonance water signal has been set to zero in order to high-light the vibration sidebands.

In addition to linearity with respect to gradient amplitude and spatial position (Fig. 5) it is also important that the vibration-related sidebands are linearly additive with respect to time. Fig. 6A and B show two separate NMR sequences with a single gradient pulse and their respective vibration-related sidebands (Fig. 6D and E) as measured on a small, spherical phantom in the magnetic isocenter. Fig. 6C shows the NMR sequence in which the two gradient pulses are present at the exact same temporal position relative to the acquisition window as in Fig. 6A and B. The temporal magnetic field perturbation and hence the vibration-related sidebands generated by the two pulse sequence (Fig. 6G) is identical to the sum of the vibration-related sidebands generated by the sequences with a single gradient pulse (Fig. 6F). This indicates that once the response of a single gradient pulse is known, the performance of an entire sequence of multiple gradient pulses can be predicted. Linear addition of temporal magnetic field perturbations also holds for gradient pulses along orthogonal directions, as well as for responses measured out of the magnetic isocenter (data not shown).

Finally, it is important that the temporal magnetic field perturbations are independent of the sample. Specific for the Bruker 4 T system at Yale, the railings that support the patient bed run directly on the bottom of the gradient coils. If the vibration-related sidebands are caused by direct vibration of the patient bed and/or RF coil assembly, it can be expected that the vibration-related sidebands are a function of the patient weight. Fig. 7A shows that this is not the case; the vibration-related sidebands measured on a small water-filled sphere mounted to an empty or a loaded (+80 kg) patient bed are identical. Further support for the observation that vibration-related sidebands are not caused by direct vibration of the patient bed and/or RF coil assembly is provided by the fact that the sidebands observed in Fig. 7A are identical when the phantom is mounted on a wooden beam which does not touch the gradient coils directly (data not shown).

5. Discussion

Here we have presented the characterization and compensation of vibration-related magnetic field perturbations. Previous work [11], as well as a large number of systematic experiments performed here have established that the associated phase modulation can be accurately described by damped sinusoidal functions. Using this functional relationship the phase modulations could be approximated, and subsequently compensated, to within the spectral noise level.

The current implementation for compensation of vibration-related magnetic field perturbations is highly specific for a given NMR pulse sequence. A more generally applicable method would calculate the temporal magnetic field perturbation for a given NMR pulse sequence from the response of a single, normalized magnetic field gradient input. Several of the more stringent requirements underlying these calculations were experimentally tested here. Firstly, the vibration-related magnetic field amplitude perturbations varied linearly with the magnetic field gradient strength, whereas the vibration-related sideband frequency, phase and decay constant were constant. A small fraction of the sidebands showed a linear dependence on spatial position, such that complete characterization and compensation of sidebands requires modulation of the first-order gradients in addition to the B_0 magnetic field. Secondly, the response of the magnetic field to a magnetic field gradient input is temporally additive. Therefore, once the response to a single, normalized gradient input is known, the response to any arbitrary gradient sequence can be calculated by simple (temporal) shifting and scaling. Of course, a generally applicable method would not be possible if the vibration-related sidebands vary with the sample under investigation. Fortunately, from the experiments presented here no correlation between sample shape, size and weight and vibration-related sidebands was observed.

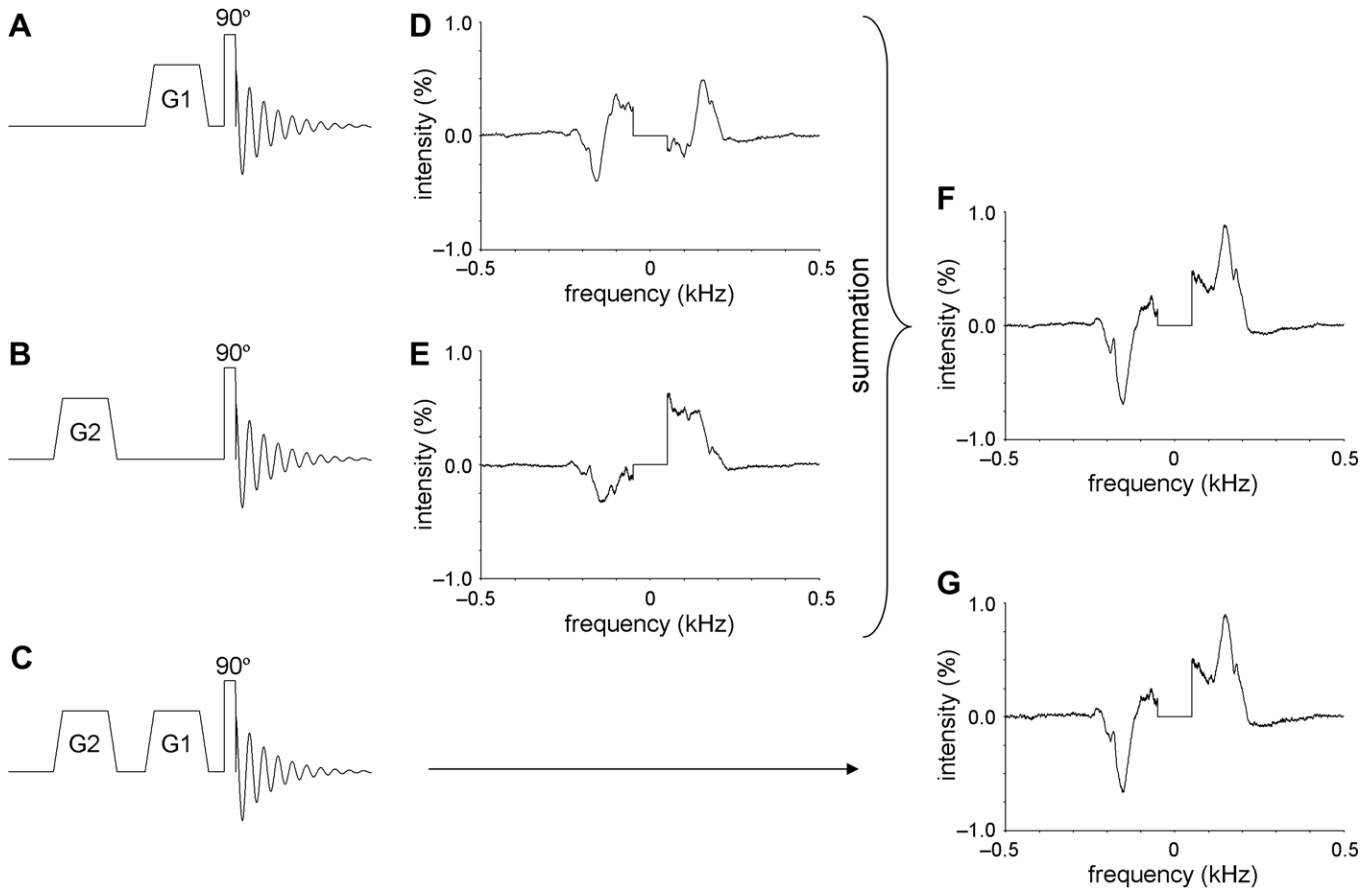

Fig. 6. (A–C) NMR pulse sequences to test the temporal linearity of vibration-related phase modulations. The magnetic field gradients G1 and G2 in (C) are identical in amplitude, duration and temporal position as those in (A) and (B). (D and E) Spectral sidebands as generated by the sequences shown in (A) and (B). Note that all spectra shown are calculated as the difference between G1/G2 $\neq 0$ and G1/G2 $= 0$. The residual on-resonance water signal has been set to zero in order to high-light the vibration sidebands. (F) Sum of (D) and (E). (G) Spectral sidebands as generated by the sequence shown in (C). The sidebands in (F) and (G) are identical to within experimental accuracy.

In fact, to obtain compensation for sidebands on the human brain *in vivo* we used the sidebands measured and quantified on a spherical phantom *in vitro*.

Given that the basic requirements are met, there are several methods by which a generic method of vibration-related sideband compensation can be implemented. With modern digital signal processing (DSP) chips, compensation of regular, exponential eddy currents is calculated in real-time. While a similar approach could also be used for the more general case of damped sinusoidal magnetic field perturbations, it remains to be demonstrated if modern DSP chips have sufficient computing power and speed to calculate 40–50 damped sinusoids within a small fraction of the spectral dwell-time. A computationally less intensive method would be to combine the currently implemented waveform memory technique with a simpler DSP algorithm. The exact magnetic field amplitude, duration and temporal position are readily extracted from the pulse sequence program, such that the temporal response of the magnetic field can be calculated prior to the experiment and stored in local memory. The response related to variable gradients, like phase-encoding or diffusion gradients, can be stored in a separate waveform memory, and following appropriate scaling, summed with the response of the constant part as the sequence is executed.

In the present study, the temporal magnetic field B_0 perturbations were minimized by feeding a compensating current into the B_0 coil. However, many clinical systems are not equipped with a B_0 coil. Fortunately, a similar level of compensation can be expected by modulating the receiver phase during acquisition and recalculating the RF phase modulation during transmission in order to track the temporally varying phase.

It should be noted that for the current application of single-volume MRS, a similar level of compensation could have been achieved through post-acquisition methods [8,9]. The B_0 magnetic field modulation could have been estimated from an *in vitro* water signal obtained with the same sequence and then applied to the *in vivo* time domain signal. However, when many different MR methods are used, or when extended acquisitions are required (e.g. MRSI, 2D NMR), the post-acquisition methods becomes time-consuming and impractical. Furthermore, in the presence of spatially varying magnetic field modulations

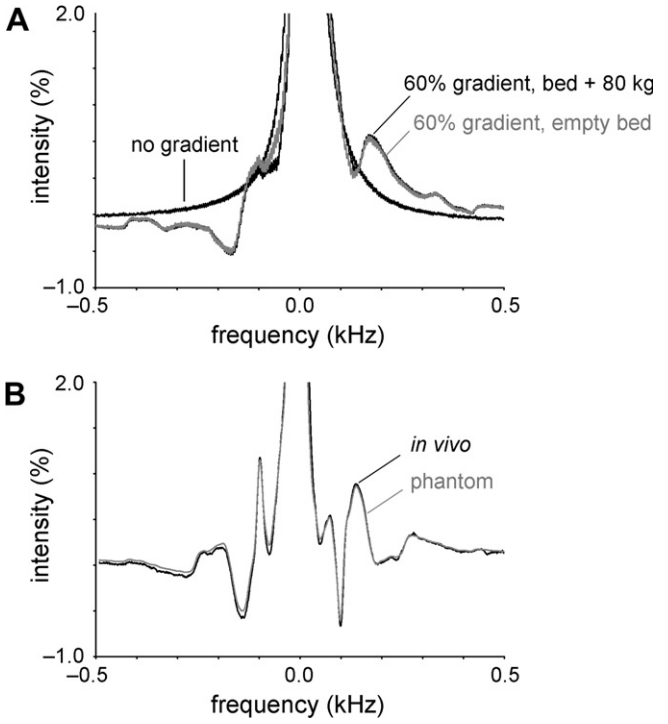

Fig. 7. Sample dependence of vibration-related sidebands. (A) The spectral sidebands measured on a small *in vitro* spherical sample mounted to an empty patient bed or a patient bed loaded with 80 kg of water bottles are identical to within experimental accuracy. (B) The spectral sidebands as measured with LASER localization on a large water sphere *in vitro* or the human brain *in vivo* are identical to within experimental accuracy. Note that the *in vitro* spectrum was broadened by circa 7 Hz in order to match the *in vitro* and *in vivo* line widths.

(Fig. 5B) post-acquisition methods can no longer provide complete compensation. In addition, post-acquisition methods only allow compensation during signal acquisition. The results presented in Figs. 5–7 indicate that a hardware-based approach can be developed that allows complete compensation that is transparent for the end-user, works for any method during the entire time span of the sequence and can compensate zero, as well as first-order spatially varying magnetic field modulations.

The immediate applications of the described method are primarily in MR spectroscopy and spectroscopic imaging. In conventional, water-suppressed MRS and MRSI the presented method will lead to greatly improved spectral line shapes, which will aid in metabolite quantification. However, even more promising is the potential for non-water-suppressed MRS and MRSI. The large water signal can be used for phase and frequency correction, internal concentration referencing and as an objective measure for accepting or rejecting spectra in large MRSI datasets. However, vibration-related sidebands overlapping with the small metabolite signals have largely prevented non-water-suppressed MRSI. The presented method reduces vibration-related sidebands to such a degree that non-water-suppressed MRSI becomes a reality. Note that while MRS on small volumes only requires B_0 magnetic field compensation, MRSI over larger volumes requires both B_0, as well as linear gradient field compensation. Dreher and Leibfritz [15] have presented a NMR-based method to separate vibration-related sidebands from metabolite signals. While very robust and easy to implement, the method requires two separate scans and is not as generally applicable as the hardware-based method presented here.

As has been shown by others [11], vibration-related NMR sidebands and acoustic noise are likely to have the same, or at least very closely related origins. As such it can be expected that some of the novel strategies to reduce the acoustic noise level will also lead to a reduction in magnetic field perturbations and hence NMR sidebands. A particularly promising approach was presented by Mansfield and coworkers in which the vibrational modes and the acoustic noise of the gradient coils were substantially reduced by using solid plates and balanced loops [22,23]. Future studies will be required to establish if this approach is also suitable for reducing vibration-related sidebands.

Acknowledgment

This research was supported by NIH Grants R21-CA118503 and R01-EB000473.

References

[1] D.J. Jensen, W.W. Brey, J.L. Delayre, P.A. Narayana, Reduction of pulsed gradient settling time in the superconducting magnet of a magnetic resonance instrument, Med. Phys. 14 (1987) 859–862.
[2] P. Jehenson, M. Westphal, N. Schuff, Analytical method for the compensation of eddy-current effects induced by pulsed magnetic field gradients in NMR systems, J. Magn. Reson. 90 (1990) 264–278.
[3] J.J. van Vaals, A.H. Bergman, Optimization of eddy-current compensation, J. Magn. Reson. 90 (1990) 52–70.
[4] G.Z. Yao, C.K. Mechefske, B.K. Rutt, Characterization of vibration and acoustic noise in a gradient-coil insert, MAGMA 17 (2004) 12–27.
[5] S.A. Counter, A. Olofsson, H.F. Grahn, E. Borg, MRI acoustic noise: sound pressure and frequency analysis, J. Magn. Reson. Imaging 7 (1997) 606–611.
[6] D.L. Price, J.P. De Wilde, A.M. Papadaki, J.S. Curran, R.I. Kitney, Investigation of acoustic noise on 15 MRI scanners from 0.2 T to 3 T, J. Magn. Reson. Imaging 13 (2001) 288–293.
[7] Y. Wu, B.A. Chronik, C. Bowen, C.K. Mechefske, B.K. Rutt, Gradient-induced acoustic and magnetic field fluctuations in a 4 T whole-body MR imager, Magn. Reson. Med. 44 (2000) 532–536.
[8] R.J. Ordidge, I.D. Cresshull, The correction of transient B_0 field shifts following the application of pulsed gradients by phase correction in the time domain, J. Magn. Reson. 69 (1986) 151–155.
[9] U. Klose, *In vivo* proton spectroscopy in presence of eddy currents, Magn. Reson. Med. 14 (1990) 26–30.
[10] P. Jezzard, A.S. Barnett, C. Pierpaoli, Characterization of and correction for eddy current artifacts in echo planar diffusion imaging, Magn. Reson. Med. 39 (1998) 801–812.
[11] D.B. Clayton, M.A. Elliott, J.S. Leigh, R.E. Lenkinski, ^{1}H spectroscopy without solvent suppression: characterization of signal modulations at short echo times, J. Magn. Reson. 153 (2001) 203–209.
[12] P.J. Bolan, L. DelaBarre, E.H. Baker, H. Merkle, L.I. Everson, D. Yee, M. Garwood, Eliminating spurious lipid sidebands in ^{1}H MRS of breast lesions, Magn. Reson. Med. 48 (2002) 215–222.

[13] L.N. Ryner, P. Stroman, T. Wessel, D.I. Hoult, J.K. Saunders, Effect of oscillatory eddy currents on MR spectroscopy, Proc. Int. Soc. Magn. Reson. Med. 6 (1998) 1903.
[14] D.B. Clayton, M.A. Elliott, R.E. Lenkinski, *In vivo* proton spectroscopy without solvent suppression, Concepts Magn. Reson. 13 (2001) 260–275.
[15] W. Dreher, D. Leibfritz, New method for the simultaneous detection of metabolites and water in localized *in vivo* ^{1}H nuclear magnetic resonance spectroscopy, Magn. Reson. Med. 54 (2005) 190–195.
[16] M.S. Ozdemir, Y. De Deene, E. Achten, Y. D'Asseler, I. Lemahieu, Quantitative proton magnetic resonance spectroscopy in the presence of sidebands, IEEE Int. Symposium Biomed. Imag. 4 (2007) 1008–1011.
[17] J.W. van Der Veen, D.R. Weinberger, G. Tedeschi, J.A. Frank, J.H. Duyn, Proton MR spectroscopic imaging without water suppression, Radiology 217 (2000) 296–300.
[18] M. Garwood, L. DelaBarre, The return of the frequency sweep: designing adiabatic pulses for contemporary NMR, J. Magn. Reson. 153 (2001) 155–177.
[19] J. Slotboom, A.F. Mehlkopf, W.M. Bovee, A single-shot localization pulse sequence suited for coils with inhomogeneous RF fields using adiabatic slice-selective RF pulses, J. Magn. Reson. 95 (1991) 396–404.
[20] R.A. de Graaf, K. Nicolay, Adiabatic water suppression using frequency selective excitation, Magn. Reson. Med. 40 (1998) 690–696.
[21] A. Haase, J. Frahm, W. Hanicke, D. Matthaei, ^{1}H NMR chemical shift selective (CHESS) imaging, Phys. Med. Biol. 30 (1985) 341–344.
[22] P. Mansfield, B. Haywood, Principles of active acoustic control in gradient coil design, MAGMA 10 (2000) 147–151.
[23] B. Haywood, B. Chapman, P. Mansfield, Model gradient coil employing active acoustic control for MRI, MAGMA 20 (2007) 223–231.